

Peg-in-Hole under State Uncertainties via a Passive Wrist Joint with Push-Activate-Rotation Function

Toshihiro Nishimura, *Student Member, IEEE*,
Yosuke Suzuki, *Member, IEEE*, Tokuo Tsuji, *Member, IEEE*, and Tetsuyou Watanabe, *Member, IEEE*

Abstract— This study presents a novel passive wrist joint with push-activate-rotation (PAR) functionality for a peg-in-hole assembly and a strategy utilizing the passivity and inherent functionality of the wrist. The PAR function involves rotation around a vertical axis, automatically activated by pushing the wrist in the vertical direction. The novel features of the approach are that 1) hardware based passive compliance absorbs uncertainties of the states for the peg, 2) no active rotational joints are required for the manipulator part, 3) F/T sensors are not used; instead, an IMU sensor is, and 4) multiple shapes for the peg or hole are available e.g., rectangular, circular, hexagonal, and triangular prisms. The validity of the approach is shown via several experiments.

I. INTRODUCTION

Peg-in-hole is one of the most fundamental assembly tasks in robotic manipulations, and much effort has been directed towards finding improved approaches [1][2][3][4][5]. Mainly, approaches for realizing practical tasks are divided into software and hardware compliances. The software-based approach utilized Force/Torque (F/T) sensory information [6][7][8][9]. Kim et al. proposed an algorithm for conducting tasks despite large positional and directional errors with F/T sensors [6]. Chung et al. realized a fixtureless peg-in-hole for a highly uncertain environment utilizing the F/T sensory information with two manipulators [7]. In [8], two types of impedance controllers were proposed for a peg-in-hole method. Jasim et al. proposed the methodology to determine the position of the hole using a force sensor [9]. Visual sensors are also popularly utilized for peg-in-hole problems [10][11][12]. Huang et al. presented a fast peg-in-hole strategy with visual compliance [10][11]. Su et al. presented a sensor-less peg-in-hole strategy for an eccentric peg such as a crankshaft based on visual information [12]. Some approaches combined F/T and visual sensors [13][14]. Song et al. presented a peg-in-hole methodology involving complex shapes with a F/T sensor and an eye-in-hand-camera [13]. Kim et al. proposed an assembly strategy where a vision system was used for pose estimation while force control was used for the procedure itself [14]. F/T information for peg-in-hole can be estimated from torque input to manipulators by an observer [15]. Polverini et al. presented a sensor-less approach based on the observer [16]. Park et al. proposed a strategy inspired by human behavior without F/T sensors [17]. Recently, they extended the strategy utilizing the

assistance of manipulators [18]. Matsuno et al. developed a trajectory switching generator with a free wrist joint for inserting a long peg into a tandem shallow hole [19]. The strategies requiring no F/T sensors [16][17][18][19] are applicable to the specified shapes of the peg and hole, while the strategies with rich information from vision and F/T sensors [13][14] can deal with several type of shapes.

Meanwhile, in industrial applications, hardware based compliance has been popular for the peg-in-hole methods since the proposal of the remote center of compliance (RCC) mechanism by Whitney [20]. With an RCC device, even a simple controller can provide fine peg-in-hole assembly. Therefore, an RCC based system is useful in practical situations. However, the RCC device is specified to one target task. Additionally, RCC can only deal with a hole on a horizontal surface, and the edge of the hole must be planed off. Yun et al. realized a two-dimensional peg-in-hole method by reinforcement learning with a 3-DOF manipulator with passive compliance joints [21]; however, there were no real experimental results. The main drawback of passive compliance devices like RCC is that the target peg and hole are specified. This might be the reason why most of the studies took the software based approach. However, a passive compliance device has merits. For example, uncertainties of the states can be reduced, F/T sensors which are usually high cost are not needed, and a controller for the device can be simple.

This study challenges a hardware based approach and develops a novel passive wrist joint (PWJ) with a push-activate-rotation (PAR) function. The PAR function involves a rotation around a vertical axis automatically activated by pushing the wrist in the vertical direction. This study also presents the procedure utilizing the PWJ and the PAR function; a) inclining the peg so that the peg can make frictional contact with two sides of the hole for the alignment while restoring elastic energy, and b) completing the insertion by activating the PAR function while utilizing the contact constraint and the restoring force. While different from conventional peg-in-hole strategies which use frictionless contact, our strategy utilizes frictional contact. It should be noted that frictional contact can be called *jamming*, which normally should be avoided in a conventional peg-in-hole assembly. This study rises to the challenge of effectively utilizing it. The other novel features of the approach are the following: 1) the passive compliance

* Research partly supported by NEDO.

T. Nishimura is with the Graduated school of Natural science and Technology, Kanazawa University, Kakuma-machi, Kanazawa, 9201192 Japan (e-mail: to.nishimura@stu.kanazawa-u.ac.jp).

Y. Suzuki, T. Tsuji, and T. Watanabe are with the Faculty of Mechanical Engineering, Institute of Science and Engineering, Kanazawa University, Kakuma-machi, Kanazawa, 9201192 Japan (e-mail: te-watanabe@iecc.org)

absorbs uncertainties of the states of the peg and hole, 2) no active rotational joints are required for the manipulator part, 3) F/T sensors are not used; rather, an IMU sensor is used, and 4) multiple shapes of the peg or hole are available, e.g., rectangular, circular, hexagonal, and triangular prisms. Different from RCC devices, the proposed system can deal with multiple shapes of chamferless hole or peg and a hole on a horizontal surface.

II. PROBLEM DEFINITION AND STRATEGIC OVERVIEW

Aiming at a simple system, this study presents a peg-in-hole assembly via an xyz automatic positioning stage shown in Fig. 1(a). Note that the system can work at normal 6 DOF manipulators if adopting the same strategy. The developed passive wrist joint and the gripper were attached to the tip of the xyz automatic positioning stage. The state and shape of the hole are given, and the edges of the hole were not planed off. A camera was utilized to identify the (initial) state of the grasped peg, but the estimation error was considered as part of the uncertainty of the state. The procedure (Fig. 1(b)) started with picking a peg, capturing the bottom face of the peg by the camera to estimate its state, and inserting the peg into the hole. The coordinates in this study were defined as shown in Fig. 1(a) where the origin was located at the geometrical center of the hole, the z axis corresponds to the normal direction of the hole or the table including the hole, and the y axis corresponds to the depth direction. The longitudinal direction of the peg was assumed to coincide with z axis at the initial state. An IMU (acceleration) sensor was attached to the gripper so that the pose of the peg/wrist could be estimated irrespective of the passive motion of the PWJ. Let θ_i ($i \in \{x, y, z\}$) be the rotation angle of the peg around the i -th axis. Without loss of generality, it is assumed that when the peg is inserted the hole, the rotation angle of the peg is $\mathbf{0}$ ($\theta_x = \theta_y = \theta_z = 0$) and the position of the peg is $\mathbf{0}$ ($x_p = y_p = z_p = 0$). It is also supposed that the initial position of the PWJ is at the right side ($x_w > 0$) where $\mathbf{p}_w = [x_w, y_w, z_w]^T$ denotes the position of the PWJ. Let θ_{z_0} be the initial θ_z and $\theta_{z_0} \leq 0$ was assumed considering the symmetry of the system. If $\theta_{z_0} > 0$, the right and left sides of the procedure only should be inverted. We will present the strategy where the posture angle between the z axis and the longitudinal direction of the peg is only required to be measured, under the assumption that the hole is known.

For convenience, we will explain the case when the shape of the bottom face of the hole and peg is a quadrangle. The key objectives for the peg-in-hole method are as follows:

- (A) To bring the peg into the state shown in Fig. 2.
- (B) To utilize frictional contact to incline the peg by translational motion.

At the state in Fig. 2, we have static frictional contacts at the left and front sides of the hole, and restored elastic energy in $-x$ and $-y$ directions. If we push the peg/PWJ in the $-z$ direction in this state, the PAR function is activated and the rotation around the z axis, which can generate a large torque, occurs. The large torque causes the static frictional contacts to become kinetic frictional contacts, and the peg rotates whilst keeping the contact with the two sides of the hole. Owing to the contact constraint and passive compliance of the PWJ, the bottom face of the peg was totally inserted into the hole. Then,

the peg was completely inserted by pushing the peg in $-z$ direction. To realize the state shown in Fig. 2, the method for inclining the peg is required, and the proposed strategy (B) is adopted. Any active rotational joints are then not required in the manipulator part.

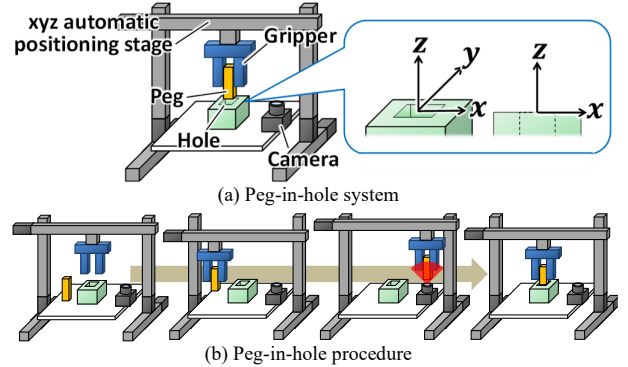


Figure 1. Peg-in-hole system and its procedure

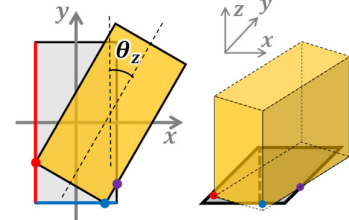


Figure 2. Key state of the peg (orange color) and hole (gray color) for completing the peg-in-hole

III. PASSIVE WRIST JOINT (PWJ) WITH PAR FUNCTION

A. Design requirements

To realize the presented strategy, the following design requirements for the PWJ were considered.

1. Positive rotation around the z axis is activated by a pushing motion in the $-z$ direction (PAR function).
2. Passive compliance is embedded in the θ_x , θ_y , and θ_z directions. Note that $\theta_x \geq 0$ to facilitate the peg-in-hole on a vertical wall.

Fig. 3 shows the structure of the developed PWJ, which was mainly constructed from a rotational shaft (in red) and a shaft bearing (light blue). The shaft bearing enables rotation around z axis. As shown in Fig. 4, the turned-up gears are attached on the rotational shaft in a circular manner. Springs bent by the wires are attached on the bearing so that the springs can contact the turned-up gears. When there is no external force, the PWJ freely rotates around the z axis. If the compression force (for example, due to the contact with a table) is applied to the PWJ in the $+z$ direction, the rotational shaft translates to contact with the springs, and the springs are likewise compressed. Because the springs are bent, the bending proceeds and the gear teeth are pushed, which causes the positive rotational motion around the z axis. By utilizing stiff springs, the rotation around the z axis can generate a large torque. This structure/mechanism is referred to as the Push-Activate-Rotation function (PAR function). If the compression force is released, the springs go to the next space of in gear teeth and

the PWJ irreversibly rotates a constant amount around the z axis. Owing to this function, the rotation can be generated without any actuators by mere contact with the table.

The shaft bearing includes a partly silicone structure (Fig. 3). Owing to the silicon parts, the PWJ rotates when the peg is caught in the hole, or the translational motion is prevented by contact friction, as shown in Fig. 5. The silicone parts were attached so that the PWJ can rotate around the $\pm y$ axis (Fig. 5(a)) while the PWJ can only positively rotate around x axis; $\theta_x \geq 0$ (Fig. 5(b)) to facilitate a peg-in-hole on a vertical wall.

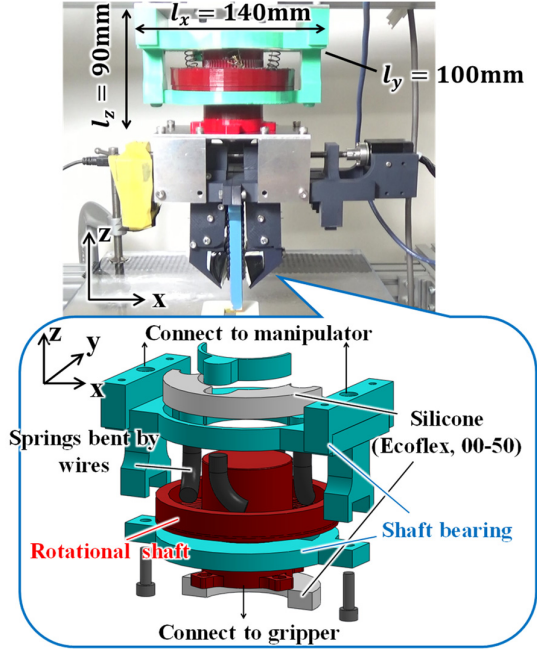


Figure 3. Schematic of the structure of the developed wrist joint. l_x , l_y , and l_z are the dimension of the wrist.

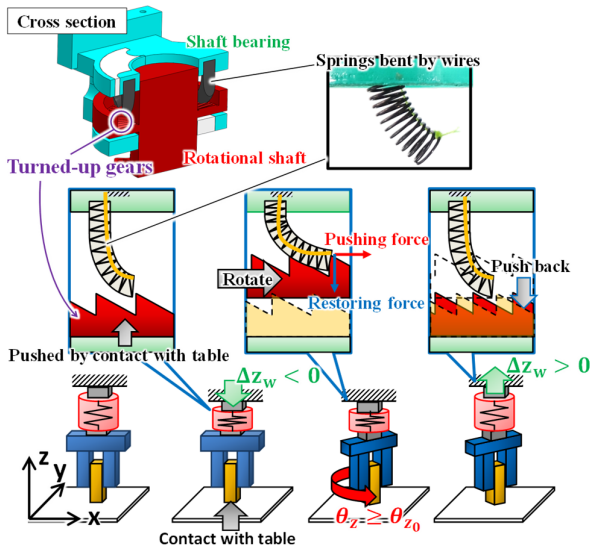


Figure 4. Schematics of the mechanism of PAR function

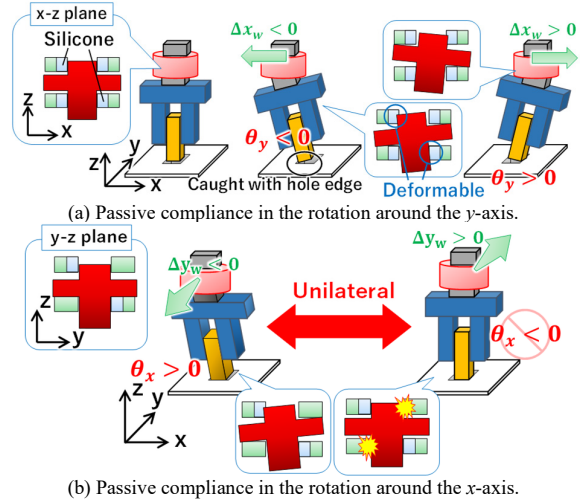


Figure 5. Passive compliance of the developed wrist joint.

B. Feasible study

In order to confirm the functionality of the PWJ, the experiments shown in Fig. 6 were conducted. The gripper holding a peg attached to the PWJ attached to the xyz automatic positioning stage was utilized.

Let $\mathbf{a}_0 \in \mathbb{R}^3$ be the output of the acceleration sensor in the initial state and $\mathbf{a}_t \in \mathbb{R}^3$ be the output at time t . In the proposed strategy, the direction for inclining the peg can be specified, and consequently, the posture angle between the z axis and the longitudinal direction of the peg θ_t provide enough information to solve for the incline. By utilizing the IMU information, \mathbf{a}_0 , and \mathbf{a}_t , θ_t is given by:

$$\theta_t = \cos^{-1} \frac{\mathbf{a}_0 \cdot \mathbf{a}_t}{|\mathbf{a}_0| |\mathbf{a}_t|} \quad (1)$$

In the experiment shown in Fig. 6(a), we examined the posture angle θ_t of the PWJ when applying a load at the tip of the peg with a force gauge (IMADA DS2-50N). Fig. 7 shows the results when the loading direction were the $-x$ and $\pm y$ directions. Note that the results when loading in the $+x$ direction can be regarded as the same as those in the $-x$ direction owing to the symmetry of the structure. Fig. 7 shows that the posture changed little when loading in the $-y$ direction while the posture substantially changed when loading in the other directions. The results revealed that the peg can be inclined by the translational motion of the PWJ, and the PWJ has the constraint of $\theta_x \geq 0$.

In the experiment shown in Fig. 6(b), we confirmed the PAR functionality of the PWJ. We examined the angle of the rotation generated by the PAR function when pushing a table with the peg. The mean angle was 28° ($\sigma = 1.9$) when the number of the tests was 5. Next, we examined the torque generated by the rotation. The peg shown in Fig. 6(b) was utilized. The force at the action point was measured by the force gauge when activating the PAR function. Fig. 8 shows a result for the relation between the pushing distance in the z direction and the torque activated by PAR function. It can be seen that when the pushing distance is within $[-8, 0]$, a passive compliance can be obtained by compressing the PWJ while the PAR function is not activated. The mean torque was 0.50 Nm ($\sigma = 3.0 \times 10^{-2}$) when the number of the tests was 5. Then,

the peg can be inserted into the hole by the activated rotational motion which can generate a large torque, even when there is a postural error around the z axis.

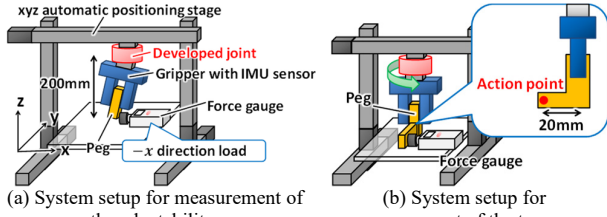


Figure 6. System setups for feasible study.

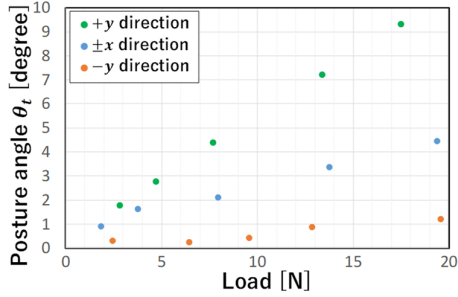


Figure 7. Load applied by the force gauge versus the posture angle θ_t .

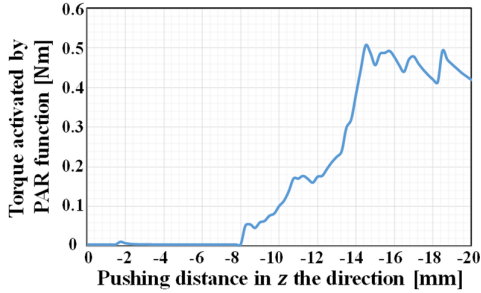


Figure 8. Pushing distance in z direction versus torque activated by PAR function

IV. PROCEDURE FOR PEG-IN-HOLE

A. System for Peg-in-Hole

For convenience, the table was constructed from a transparent acrylic and the camera was set to observe the peg on the table. The posture of the peg around the z axis (on the x - y plane) was estimated by the camera image (See Fig. 9).

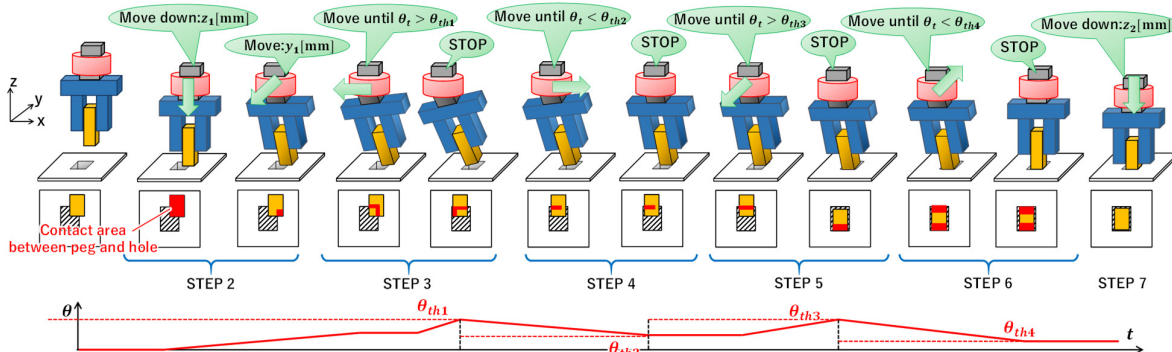


Figure 10. Schematics of the peg-in-hole procedure and time series data of the posture angle θ_t

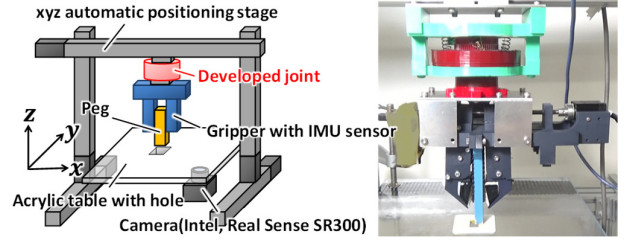


Figure 9. Schematic view of the system setup in this study.

B. Procedure

Based on the proposed strategy given in Section II, we were challenged to produce the procedure including the following features as procedure requirements:

1. The same procedure is applicable to different shapes of pegs and holes.
2. F/T sensors are not needed, with only θ_t given at (1) derived from IMU sensory information needed.
3. Postural error around the z axis is removed by the PAR function.
4. Positioning and postural errors are allowed.

For convenience, the procedure for a rectangular prism is presented as a representative procedure (Fig. 10). Here, the point of the peg that is first inserted into the hole is referred to as the First-Insertion point (FI point). At the initial state, the lowest point of the bottom face of the peg in the x direction is selected as the FI point. If there are multiple lowest points, the lowest point in the y direction is selected as the FI point.

Step 1) Move the PWJ to the initial position $\mathbf{p}_{w_0} = [x_0, y_0, z_0]^T$ (How to determine the \mathbf{p}_{w_0} is described in the next subsection).

Step 2) Move the PWJ downward in the $-z$ direction such that $z_w = z_1 (< 0)$, which is determined so that a passive compliance can be obtained by compressing the PWJ while the PAR function is not activated. After that, we move it in the $-y$ direction with an increment of $y_1 (> 0)$ (see the next subsection for the definition of y_1). Then, the contact between the peg and the table becomes a line contact.

Step 3) Move the PWJ in the $-x$ direction with a constant speed of v . The peg tilts and the FI point is inserted into

the hole or becomes a point-contact point. In both cases, the contact friction prevents the translational motion. If the lateral force due to the input for the lateral motion is greater than the frictional force, the peg starts sliding on the table. If the FI point goes into the region of the hole (the hatching area in Fig. 10), the peg is caught by the hole. After that, the peg moves in the caught state, and then θ_t increases. When θ_t reaches the threshold θ_{th1} , we judge that contact with the edge of the hole has occurred and stop the motion. The contact point is referred to as First-Contact point (FC point) (red point in Fig. 11). The edges of the peg and hole including the FC point are respectively referred to as FCp and FCh edges. The operation is for the insertion of the FI point and the alignment between the FCp and FCh edges (at the left-side edge of the hole). The energy is restored at the PWJ. It is noted that the position of the FC point on the FCp and FCh edges change with the subsequent operations.

Step 4) Move the PWJ in the $+x$ direction with a constant speed of v . Owing to the release of the restored energy at the PWJ, the inclination of the peg decreases, and the peg becomes close to a standing-up posture. We stop the motion when θ_t reaches the threshold θ_{th2} . By this operation, the vertex of the peg, whose y -coordinate value is the lowest, is inserted into the hole.

Step 5) Move the PWJ in the $-y$ direction with a constant speed of v . Similar to Step 3, the peg first inclines and then slides. If the peg is caught by the edge of the hole, θ_t increases. When θ_t reaches the threshold θ_{th3} , we judge that contact with the (front) edge of the hole has occurred, and consequently stop the motion. The contact point is referred to as the second-contact point (SC point) (blue point in Fig. 11). The edges of the peg and hole including the SC point are respectively referred to as SCp and SCh edges. The alignment between the SCp and SCh edges is realized (at the front side edge of the hole). The energy is restored at the PWJ.

Step 6) Move the PWJ in the $+y$ direction with a constant speed of v . Owing to the release of the restored energy at the PWJ, the inclination of the peg decreases, and the peg becomes close to a standing-up posture. We stop the motion when θ_t reaches the threshold θ_{th4} . The state shown in Fig. 2 is then realized.

Step 7) Move the PWJ downward in the $-z$ direction. The peg rotates around the z axis owing to the PAR functionality. The rotation around the z axis is constrained by the FCh and SCh edges, and the bottom face of the peg is completely inserted into the hole. From this state, the peg is completely inserted into the hole by pushing the peg in the $-z$ direction.

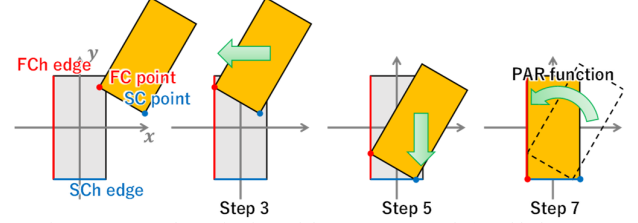


Figure 11. Schematic view of the peg (orange color) and hole (gray color), when the orientation of the peg does not correspond to that of the hole at the initial state; $\theta_{z_0} < 0$ (Case II).

Here, the method to tune θ_{thi} is presented. θ_{th1} and θ_{th3} are thresholds for detecting a contact with the edge of the hole. The values should be large enough not to incorrectly detect stick-slip, but to accurately detect the contact. We measured the values at the tests three times and tuned the values. θ_{th2} and θ_{th4} are the thresholds for getting the peg back to standing-up posture. The requirement for the tuning is to keep the contacts at the FC and SC points, which have been obtained in the previous steps. Here, we show the determination method for θ_{th2} . θ_{th4} can be turned similarly to θ_{th2} . Fig. 12 shows the time-series data of θ_t when moving the PWJ in the $+x$ direction with a constant speed of v ($= 3$ mm/s) in Step 4, although we did not stop the motion with a threshold. The peg stood up when $\theta_t \cong 1.5^\circ$. After that, the contact at the FC point was lost and the contact point moved from the left to the right side. We conducted the same tests three times and found the θ_{th2} where the contact at the FC point is not always lost while the peg is close to the standing-up posture as much as possible. It is remarked that as it can be seen, each step needs not three-dimensional postural information of the peg but only θ_t , and then the acceleration sensor is only required.

The operation at Step 6 has a risk of preventing the insertion and converge at $\theta_x = 0$, namely jamming, but this is always avoided. Proof is shown in the appendix.

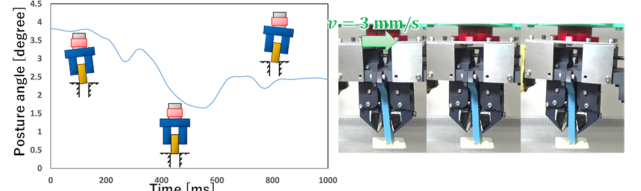


Figure 12. Time-series data of the posture angle θ_t when moving the PWJ in the $+x$ direction with constant speed (3 mm/s) at Step 4, although we did not stop the motion with a threshold.

C. Determination of the initial position

The initial position must be set so that FI point of the peg can be inserted into the hole in Step 3. In Step 2, the peg is inclined by the translation in the $-y$ direction. Therefore, at the sliding motion in the $-x$ direction in Step 3, the peg also slides in the $-y$ direction (Fig. 13). Let $y_1 (> 0)$ be the maximum amount of the sliding, which was practically examined in multiple experiments. Let $[y_{hmin}, y_{hmax}]$ be the range of y for the area of the hole. Then, the y coordinate value of the initial point should be in the interval $[y_{hmin} + y_1, y_{hmax}]$. Expressing the area of the hole by H_A , we define the area U :

$$U = \{\mathbf{P}_U = [x_U, y_U]^T | \mathbf{P}_U \in H_A, y_U \in [y_{hmin} + y_1, y_{hmax}]\}$$

U is the hole area where the FI point should be positioned at Step 1, considering the sliding in the $-y$ direction in Step 3.

The bottom face of the peg is supposed to be captured by the camera. Let $\mathbf{p}_{\text{FI}_{\text{cap}}} = [x_{\text{FI}_{\text{cap}}}, y_{\text{FI}_{\text{cap}}}]^T$ be the FI point at the captured image (bottom face). Let $\mathbf{p}_{\text{w}_{\text{cap}}} = [x_{\text{w}_{\text{cap}}}, y_{\text{w}_{\text{cap}}}, z_{\text{w}_{\text{cap}}}]^T$ be the position of the PWJ when capturing the image for the bottom face of the peg. Then, we set the initial point \mathbf{p}_{w_0} as follows (Fig. 14):

$$\mathbf{p}_{\text{w}_0} = [x_{\text{w}_{\text{cap}}} + x_{\text{U}g} - x_{\text{FI}_{\text{cap}}}, y_{\text{w}_{\text{cap}}} + y_{\text{U}g} - y_{\text{FI}_{\text{cap}}}, z_{\text{w}_{\text{cap}}}]^T$$

where $\mathbf{p}_{\text{U}g} = [x_{\text{U}g}, y_{\text{U}g}]^T$ denotes the geometric center of the area U . By this setting, we maximize the possibility of the success of the first insertion of the FI point.

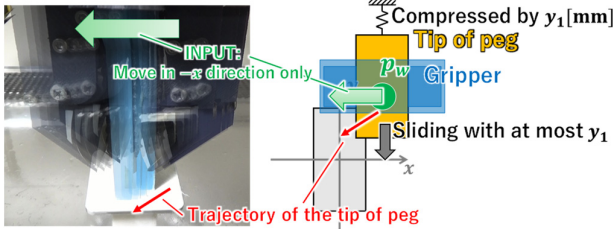
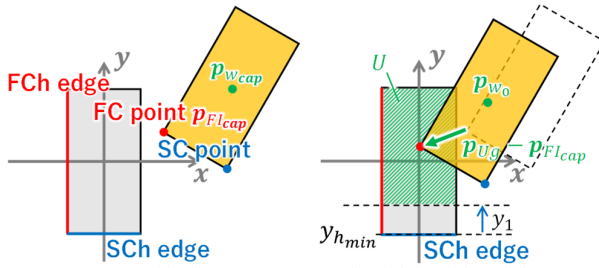


Figure 13. Sliding in the y direction when the PWJ moves in the $-x$ direction



(a) State captured by the camera (b) Initial position of the peg
Figure 14. Selection of the initial position of the peg (orange color)

V. EXPERIMENTAL VALIDATIONS

To evaluate the presented PWJ and procedure (strategy), several experimental tests were conducted. The parameters used in the experiments were as follows: $y_1 = 7$ mm, $z_1 = -3$ mm, $z_2 = 20$ mm, $v = 3$ mm/s, $\theta_{th1} = 3.5^\circ$, $\theta_{th2} = 1.4^\circ$, $\theta_{th3} = 4.5^\circ$, and $\theta_{th4} = 1.4^\circ$. The clearance of the hole was set to be 0.1 mm.

A. Peg-in-hole without postural error around the z direction

We conducted the peg-in-hole tests when the initial posture of the peg coincided with the posture of the hole ($\theta_{z_0} = 0^\circ$). The shapes and initial states of the bottom face of the target pegs are shown in Fig. 15. There were five types of shape, and the tests were conducted with eight patterns of the peg/hole orientation because different orientations of quadrangular and triangular peg/hole can have different results. All peg/holes were chamferless. The tests were started from the state where the peg was picked. The initial position was determined by the method given in Section IV.C, and the procedure described in Section IV was performed. The tests were conducted 3 times

for each peg/hole number. The peg-in-hole tasks were successful for all numbers except for No. 7. When trying No. 7, the FI point was not inserted at Step 3 because of a small inclination of the peg, and thus, the operation failed. Fig. 16 shows the time-series data of the posture angle θ_t at No.1.

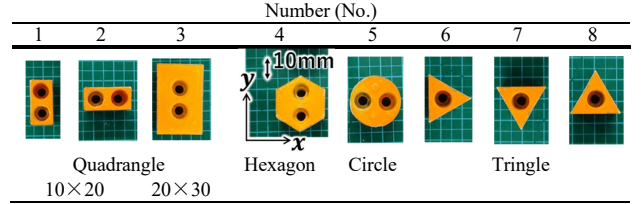


Figure 15. Pegs used in the experiment and their initial states when $\theta_{z_0} = 0$. The shape and orientation of the hole corresponds to each number of the peg.

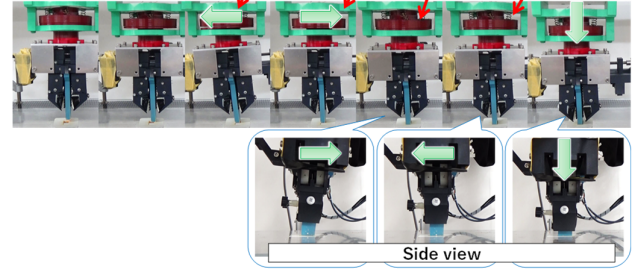
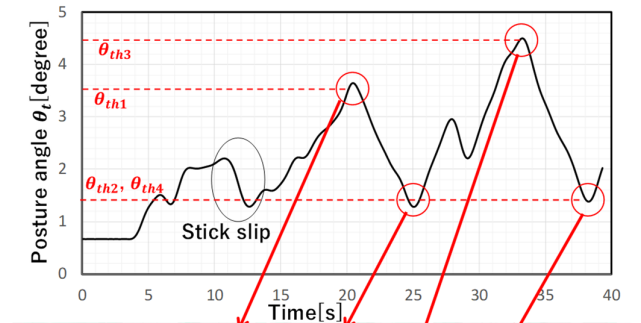


Figure 16. Time-series data of the posture angle θ_t with the procedure for No.1 peg.

B. Peg-in-hole with initial postural uncertainties around the z axis

Here, we conducted peg-in-hole experiments where the initial orientation of the peg did not correspond to the orientation of the hole ($\theta_{z_0} < 0$). The target pegs were No.1, 2, 3, 4, and 6 in Fig. 15. The experimental procedure was as follows: 1) The peg was randomly placed on the table. 2) The orientation angle of the peg $|\theta_{z_0}|$ was measured by the camera. 3) The initial position \mathbf{p}_{w_0} for the PWJ was determined by the method given in Section IV.C. 4) The procedure for the peg-in-hole operation was performed. The results were investigated by splitting the range of $|\theta_{z_0}|$ ($0-50^\circ$) into incremental ranges each spanning 5° ($0-5, 5-10, \dots$). We repeated the examinations until the number of trial times for each range was over three. Fig. 17 shows the success rate. It can be seen that if the angle $|\theta_{z_0}|$ was under 30° , the success rate was 100%, except for No. 2. The (absolute) rotational angle activated by the PAR function is 28° on average (see section III.B), and it is hard to compensate $|\theta_{z_0}| > 28^\circ$. Note that the angle of 28° depends on the tooth interval of the gear as well as the stiffness of the springs. Note also that when the rotational angle is more than 28° , compression release of the PWJ is required.

Therefore, if the angle $|\theta_{z_0}|$ was over 30° , the success rate drastically decreased. In the case of No. 2, the vertex of the peg was not inserted at Step 4. This was also true for No. 6. Instead, SC point was obtained at the end of Step 4. The difference depends on whether different FC and SC points can be obtained at the end of Step 5. Different FC and SC points were obtained for No. 6 while they were not for No.2 because the length between FC and SC points at the end of Step 4 was large for No.6 and small for No. 2 (see Fig. 18). The length decreased during the translation in Step 5. Step 5 has a role in stopping the sliding and achieving static frictional contact. For No. 2, FC and SC points became one contact point, and the peg was not constrained as expected. Hence, the subsequent procedures failed. Meanwhile, for No. 6, the contact points did not unify, and the constraints of the peg were as expected at the end of Step 5. Therefore, the subsequent procedures worked well.

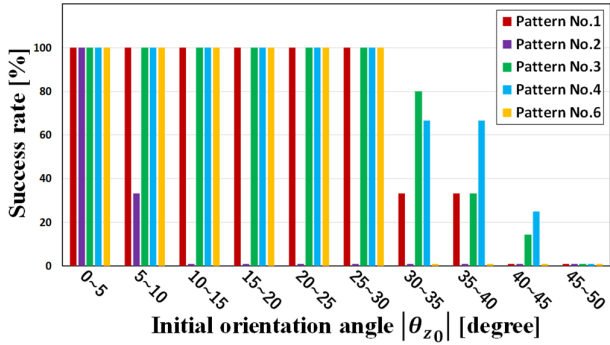


Figure 17. Initial orientation angle ($|\theta_{z_0}|$) measured by the vision sensor versus the success rate of the peg-in-hole operation.

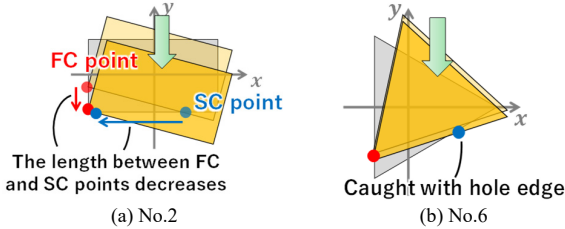


Figure 18. The length between FC and SC points at Step 5

C. Procedure for real-world situation

In this section, we present the procedure for a real-world situation where a randomly located peg is picked and inserted into the hole. When the initial posture angle for the picked peg $|\theta_{z_0}|$ is under 28° , the procedure described in Section IV is adapted. When the angle $|\theta_{z_0}|$ is over 28° , the PAR functionality was activated and the compression was released so that $|\theta_{z_0}|$ can be under 28° before continuing. After that, the procedure for the peg-in-hole operation was performed. Fig.19 illustrates a summary of the control schema for a peg-in-hole operation in an uncertain environment. The experiment in this section evaluated the usefulness of the control schema and the robustness to uncertainties caused by vision processing and picking. The No. 1 peg was used in this test. First, the peg was placed in a position sufficiently distant from the hole shown in Fig. 20. To evaluate the robustness for position uncertainty, the experiments was conducted with 5 different positions of peg; $[x_{peg}, y_{peg}]^T$, $[x_{peg}, y_{peg} \pm 1 \text{ mm}]^T$ and $[x_{peg}, y_{peg} \pm 2 \text{ mm}]^T$, where $[x_{peg}, y_{peg}]^T$ was randomly selected from the

operation range of the PWJ. The gripper picked the peg at $\mathbf{p}_w = [x_{peg}, y_{peg}, 0]^T$, which indicates there could be a positional error when picking the peg. The experiments were conducted with the initial orientation angles ($|\theta_{z_0}|$) of 0, 15 and 45° for each position of the peg. The tasks succeeded for all positions and angles. Fig. 20 shows the example where the peg's position was $[x_{peg}, y_{peg}]^T$ and the initial orientation angle ($|\theta_{z_0}|$) was 45° . If the initial angle was over 28° , then the PAR functionality was activated by releasing the compression force after the activation. After that, the presented procedure was performed to complete the insertion.

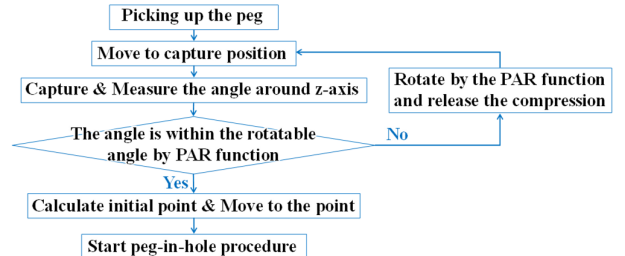


Figure 19. Control schema for peg-in-hole in real situation

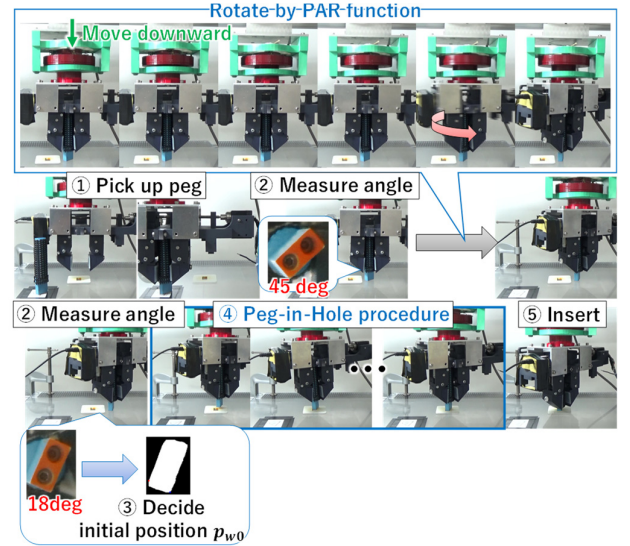


Figure 20. Peg-in-hole assembly in a real-world situation for the No. 1 peg when $\theta_{z_0} = 45^\circ$ and the initial position was randomly selected.

D. Verification of procedure requirements

The first experiment showed that the presented procedure can be applied to different shapes of the peg and hole, although the procedure did not work for the peg No. 7 (a limitation). Even for different shapes of the peg and hole, Steps 1–5 provided the alignments at the left and front edges of the hole, and brought the peg into the state shown in Fig. 2. Therefore, the presented procedure worked for the different shapes of the peg. In other words, the presented approach is valid for shape uncertainties. Requirements 2 and 3 were obviously satisfied. Requirement 4 was validated by the third experiment. In all, we concluded that the passive compliance and the PAR function provided the realization of the assembly under state uncertainties. Additionally, the assembly with the clearance of 0.1 mm was realized. Lastly, the unilateral passive compliance of the PWJ facilities a peg-in-hole on a vertical wall. Please

refer to our video-clip for an actual test result. We adopted the same strategy with the same parameters as the one given at the previous subsection.

VI. CONCLUSION

This study developed a novel passive wrist joint with Push-Activate-Rotation (PAR) function for a peg-in-hole operation with state uncertainties for the peg. A novel strategy utilizing a passive joint and PAR functionality was also proposed for the peg-in-hole. No active rotational joints were required for the manipulator part for realization. We did not utilize force/torque sensors; instead, an IMU sensor was used to estimate the initial posture of the peg during the assembly. The archived clearance of the hole was 0.1 mm. With the same procedure, we succeeded in realizing different shaped pegs with rectangular, circular, hexagonal, and triangular bottoms. The validity of the proposed wrist joint and strategy was validated by several experiments. The increased rate of the assembly process and the further investigation of the potential of the developed passive wrist joint will be included in our future work.

APPENDIX

Fig. 21 shows the low-dimensionalized model for the analysis at Step 6. Here we can assume:

$$F_v = kd \quad (2)$$

where F_v is force applied by the compressed PWJ, k is spring constant of the PWJ and d is the compression quantity of the PWJ. When the peg is translated in the $+y$ direction, two cases can occur: either the right contact point shown in Fig. 21 slides, or it does not slide. In the former case, the peg is inserted. In the latter case, d is increased by the translation, and then F_v is also increased to overcome maximum static frictional force. This causes sliding at the contact point. Therefore, the insertion proceeds without jamming at Step 6. It should be noted that even when the bottom contacts with the right corner and jamming occurs, the inclination of the peg can decrease owing to the compression of PWJ.

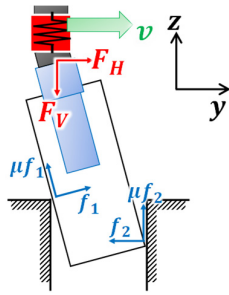


Figure 21. Schematic view for jamming analysis in Step 6.

REFERENCE

- [1] H. Bruyninckx, S. Dutre, and J. De Schutter, "Peg-on-hole: a model based solution to peg and hole alignment," in *Proceedings of 1995 IEEE International Conference on Robotics and Automation*, 1995, vol. 2, pp. 1919–1924.
- [2] T. Lozano-Perez, M. T. Mason, and R. H. Taylor, "Automatic synthesis of fine-motion strategies for robots," *Int. J. Rob. Res.*, vol. 3, no. 1, pp. 3–24, 1984.
- [3] S. R. Chhatpar and M. S. Branicky, "Search strategies for peg-in-hole assemblies with position uncertainty," in *Proceedings 2001 IEEE/RSJ International Conference on Intelligent Robots and Systems. Expanding the Societal Role of Robotics in the the Next Millennium (Cat. No.01CH37180)*, 2001, vol. 3, pp. 1465–1470.
- [4] K. Kosuge and M. Shimizu, "Planar parts-mating using structured compliance," in *Proceedings 2001 IEEE/RSJ International Conference on Intelligent Robots and Systems. Expanding the Societal Role of Robotics in the the Next Millennium (Cat. No.01CH37180)*, 2001, vol. 3, pp. 1477–1482.
- [5] B. Kim, B. Yi, I. H. Suh, and S. Oh, "Stiffness analysis for effective Peg-In / Out-Hole Tasks Using Multi-fingered Robot Hands," *IEEE Int. Conf. Intell. Robot. Syst.*, vol. 2, pp. 1229–1236, 2000.
- [6] In-Wook Kim, Dong-Jin Lim, and Kab-Il Kim, "Active peg-in-hole of chamferless parts using force/moment sensor," in *Proceedings 1999 IEEE/RSJ International Conference on Intelligent Robots and Systems. Human and Environment Friendly Robots with High Intelligence and Emotional Quotients (Cat. No.99CH36289)*, 1999, vol. 2, pp. 948–953.
- [7] Seong-Youb Chung and L. Doo Yong, "Discrete event systems approach to fixtureless peg-in-hole assembly," in *Proceedings of the 2001 American Control Conference. (Cat. No.01CH37148)*, 2001, vol. 6, pp. 4962–4967 vol.6.
- [8] T. Tsumugiwa, A. Sakamoto, R. Yokogawa, and K. Hara, "Switching control of position/torque control for human-robot cooperative task - human-robot cooperative carrying and peg-in-hole task," in *2003 IEEE International Conference on Robotics and Automation*, 2003, vol. 2, pp. 1933–1939.
- [9] I. F. Jasim, P. W. Plapper, and H. Voos, "Position Identification in Force-Guided Robotic Peg-in-Hole Assembly Tasks," *Procedia CIRP*, vol. 23, pp. 217–222, 2014.
- [10] S. Huang, K. Murakami, Y. Yamakawa, T. Senoo, and M. Ishikawa, "Fast Peg-and-Hole Alignment Using Visual Compliance," in *IEEE International Conference on Intelligent Robots and Systems (IROS)*, 2013, vol. Novenver, pp. 286–292.
- [11] Shouren Huang, Y. Yamakawa, T. Senoo, and M. Ishikawa, "Realizing peg-and-hole alignment with one eye-in-hand high-speed camera," in *2013 IEEE/ASME International Conference on Advanced Intelligent Mechatronics*, 2013, pp. 1127–1132.
- [12] J. Su, H. Qiao, Z. Ou, and Y. Zhang, "Sensor-less insertion strategy for an eccentric peg in a hole of the crankshaft and bearing assembly," *Assem. Autom.*, vol. 32, no. 1, pp. 86–99, Feb. 2012.
- [13] H.-C. Song, Y. Kim, and J. Song, "Guidance algorithm for complex-shape peg-in-hole strategy based on geometrical information and force control," *Adv. Robot.*, vol. 30, no. 8, pp. 552–563, Apr. 2016.
- [14] Y. Kim, H.-C. Song, and J. Song, "Hole detection algorithm for chamferless square peg-in-hole based on shape recognition using F/T sensor," *Int. J. Precis. Eng. Manuf.*, vol. 15, no. 3, pp. 425–432, Mar. 2014.
- [15] A. de Luca and R. Mattone, "Sensorless Robot Collision Detection and Hybrid Force/Motion Control," in *Proceedings of the 2005 IEEE International Conference on Robotics and Automation*, 2005, pp. 999–1004.
- [16] M. P. Polverini, A. M. Zanchettin, S. Castello, and P. Rocco, "Sensorless and constraint based peg-in-hole task execution with a dual-arm robot," in *2016 IEEE International Conference on Robotics and Automation (ICRA)*, 2016, pp. 415–420.
- [17] H. Park, J. Bae, J. Park, M. Baeg, and J. Park, "Intuitive Peg-in-Hole Assembly Strategy with a Compliant Manipulator," *Robot. (ISR)*, 2013 44th Int. Symp., pp. 3–7, 2013.
- [18] H. Park, J. Park, D. Lee, J. Park, M. Baeg, and J. Bae, "Compliance-Based Robotic Peg-in-Hole Assembly Strategy without Force Feedback," *IEEE Trans. Ind. Electron.*, no. 99, pp. 1–1, 2017.
- [19] T. Matsuno, T. Fukuda, and Y. Hasegawa, "Insertion of long peg into tandem shallow hole using search trajectory generation without force feedback," in *IEEE International Conference on Robotics and Automation, 2004. Proceedings. ICRA '04. 2004*, 2004, vol. 2, no. April, pp. 1123–1128 Vol.2.
- [20] D. E. Whitney, "Quasi-Static Assembly of Compliantly Supported Rigid Parts," *J. Dyn. Syst. Meas. Control*, vol. 104, no. 1, p. 65, 1982.
- [21] Seung-kook Yun, "Compliant manipulation for peg-in-hole: Is passive compliance a key to learn contact motion?," in *2008 IEEE International Conference on Robotics and Automation*, 2008, pp. 1647–1652.